Structure and properties of Titanium–25 Niobium–*x* iron alloys

C. M. LEE, W. F. HO, C. P. JU, J. H. CHERN LIN*
Department of Materials Science and Engineering, National Cheng-Kung University, 70101 Tainan, Taiwan, ROC
E-mail: chernlin@mail.ncku.edu.tw

The present work studies the effect of iron on microstructure, mechanical properties and corrosion behavior of Ti–25Nb based system with emphasis on improving strength/modulus ratio. Experimental data shows that cast Ti–25Nb–3Fe has a β phase with a entirely of dendrite morphology. The bending strength/modulus ratio is 24.6 higher than Ti–6Al–4V (17.4) by 41.4% and than c.p. Ti (9.3) by 165%. The critical anodic current density of the metal in 37 °C Hank's solutions is lower than approximately 100 $\mu A/cm^2$. Ti–25Nb–3Fe alloy has a great potential for use as an implant material.

1. Introduction

Titanium has been studied for use as an implant material as early as the 1940s [1]. Due to their low density, excellent biocompatibility, corrosion resistance and mechanical properties, pure titanium and titanium alloys are widely used for many biomedical applications today. For example, pure titanium is being used for hip cup shells, dental crowns and bridges, endosseous dental implants and plates for oral maxillofacial surgery, while high strength Ti–6Al–4V alloy is used for anchorage stem of femoral components [2].

Although Ti–6Al–4V ELI is widely used as an orthopaedic implant material due to its excellent corrosion resistance and mechanical properties, studies have shown that the release of aluminum and particularly vanadium ions from the alloy might cause some long-term health problems, such as peripheral neuropathy, osteomalacia and Alzheimer diseases [3–6]. For this reason Al, V-free titanium alloys, such as Ti–Sn–Nb–Ta–Pd [7], Ti–Nb–Zr [8], Ti–Mo–Zr–Fe [9], Ti–15Mo [10] and Ti–Mo–Hf [11], have been developed. Although these Al, V-free Ti alloys exhibited better biocompatibility and reduced moduli of elasticity (only about half that of 316L or Co–Cr–Mo), their moduli (200–240 GPa) are still 4–10 times that of human bone [12, 13].

Long-term studies indicate that insufficient load transfer from artificial implant to adjacent remodeling bone may result in bone resorption and eventual loosening of the prosthetic device [14, 15]. This phenomenon, termed ''stress shielding effect'', is a direct result of the stiffness mismatch between implant material and surrounding natural bone [16–19]. Finite element analysis suggested that a lower modulus hip prosthesis better similates the natural femur in distributing stress to the adjacent bone tissue [20, 21]. Animal study also suggested that bone remodeling commonly experienced by hip prothesis patients may be reduced by a prothesis having a lower modulus [22, 23].

Lee *et al*. [24] have recently investigated a series of binary Ti–Nb alloys with Nb contents up to 35 wt %. They found that properties of the alloys were sensitive to their crystal structure/morphology, that in turn was closely related to the Nb contents of the alloys. The alloys containing 15 wt % or less Nb were dominated by a hexagonal α' phase with an acicular, martensitic structure. The alloys containing 17.5–25 wt % Nb were primarily comprised of an orthorhombic α'' phase. With Nb contents higher than 30 wt %, the equi-axed β phase was almost entirely retained. The Ti–Nb system has demonstrated a great potential for use as an implant material in its favorable combination of high strength and modulus. For example, the binary Ti–25 wt % Nb had a bending strength of 1650 MPa and bending modulus of 77 GPa, that gave a bending strength/modulus ratio (an indication of feasibility for use as implant material) as large as 21.4. As a comparison, grade II c.p. Ti and Ti–6Al–4V have bending strength/modulus ratios of 9.29 and 17.4, respectively.

The present work is a study of the effect of iron on the microstructure, mechanical properties and corrosion behavior of Ti–25Nb based system with an emphasis on further improvement in strength/modulus ratio. The selection of iron was based on the fact that iron is one of the strongest β phase stabilizer and has demonstrated its significant influence on properties of other titanium alloy systems (Chern Lin *et al*., unpublished research).

*Author to whom all correspondence should be addressed.

2. Experimental procedure

The series of Ti–25Nb–*x*Fe alloys with Fe contents from 1 to 7 were prepared from titanium, niobium and iron each of 99.9% in purity using a commercial arc-melting vacuum-pressure type casting system (Castmatic, Iwatani Corp., Japan). This casting system consists of an upper melting chamber and lower casting chamber, both of which are connected by a central hole with each other. A casting ring is set at the bottom of the hole and a copper crucible lies on top of it. The alloy ingot is placed at the center of the crucible.

Prior to melting, the melting chamber was evacuated and purged with argon. An argon pressure of $1.5\,kgf/cm^2$ was maintained during melting. To help homogeneity, the ingot was arc-melted three times. Prior to casting, the ingot was melted again in an open-based copper hearth under argon atmosphere. The difference in pressure between the two chambers allowed the molten alloy to quickly drop into a room-temperature graphite mold as soon as the alloy was melted. Compositions of the series of cast Ti–Nb–Fe alloys determined by scanning electron microscopy/energy dispersive spectrometry (SEM/EDS) are listed in Table I.

Surfaces of the cast alloys for microstructural study were mechanically polished via a standard metallographic procedure to a final level of 0.05 μm alumina powder, then etched in a solution of water, nitric acid, and hydrofluoric acid (80 : 15 : 5 in volume). Microstructure of the etched alloys was examined using an optical microscope (MC80, Zeiss, Germany). X-ray diffraction (XRD) for phase analysis was conducted using a Rigaku diffractometer (Rigaku D-max IIIV, Rigaku Co., Tokyo, Japan) operated at 30 kV and 20 mA. A Ni-filtered CuK_α radiation was used for the study. The various phases were identified by matching each characteristic peak with the JCPDS files.

The microhardness of polished alloys was measured using a Matsuzawa MXT70 microhardness tester at a load of 200 g for 15 s. Three-point bending tests were performed using a desk-top mechanical tester (Shimadzu AGS-500D, Tokyo, Japan). The bending strengths were determined using the equation, $\sigma = 3PL/2bh^2$ [25]. The moduli of elasticity in bending were calculated from the load increment and the corresponding deflection increment between two points on a straight line as far apart as possible using the equation, $E = L^3\Delta P/4bh^3\Delta\delta$ [25]. Average bending strengths and moduli were obtained from at least five tests for each condition.

Potentiodynamic polarization of the alloys was performed using an EG&G-253 potentiostat in Hank's solution (Table II). The body temperature, 37 °C, was maintained throughout the experiment. A saturated calomel electrode (SCE) was used as reference and a platinum electrode as a counter. After a potential of − 1000 mV (SCE) had been applied to the tested alloy for 6 min, the polarization scan was started from − 800 mV (SCE) at a scan rate of 1 mV/s toward anodic direction.

TABLE I EDS-determined alloy compositions for the study

Alloy code	EDS determined composition (wt %)		
	Nb	Fe	Ti
Ti–25Nb	24.09	—	Balance
Ti–25Nb–1Fe	24.45	1.50	Balance
Ti–25Nb–3Fe	24.29	3.75	Balance
Ti–25Nb–5Fe	24.11	5.08	Balance
Ti–25Nb–7Fe	23.85	7	Balance

TABLE II Composition of Hank's solution

Constituent	g/L
NaCl	8.00
$CaCl_2$	0.14
KCl	0.40
$NaHCO_3$	0.35
Glucose	1.00
$MgCl_2 \cdot 2H_2O$	0.10
Na_2HPO_4	0.06
KH_2PO_4	0.06
$MgSO_4 \cdot 7H_2O$	0.06

3. Results and discussion

XRD patterns of the series of cast Ti–Nb–Fe alloys are shown in Fig. 1. The binary Ti–25Nb alloy showed a typical orthorhombic, α″ crystal structure. When 1 wt % Fe was added, the formation of α″ phase was suppressed and the high temperature bcc structure, β phase was almost entirely retained. The XRD patterns of higher Fe alloys were similar to that of 1 wt % Fe alloys. Due to the smaller atomic radius of Fe (1.72 Å) than Ti (2.00 Å) and Nb (2.08 Å), the addition of iron caused the β phase lattice parameters to decrease, that in turn caused the XRD peaks to shift toward high angle side. The higher the iron content, the more obvious the shift was, as shown in the XRD patterns.

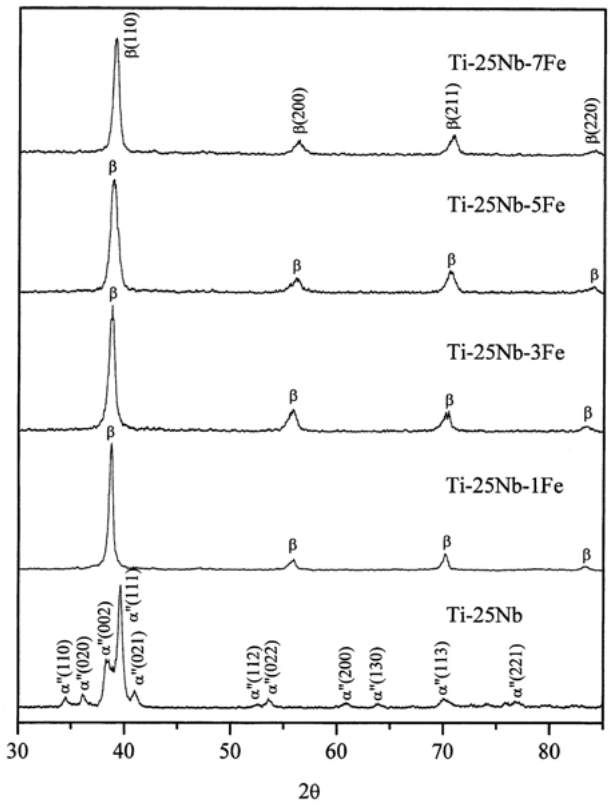

Figure 1 XRD patterns of Ti–25Nb and Ti–25Nb–*x*Fe alloys.

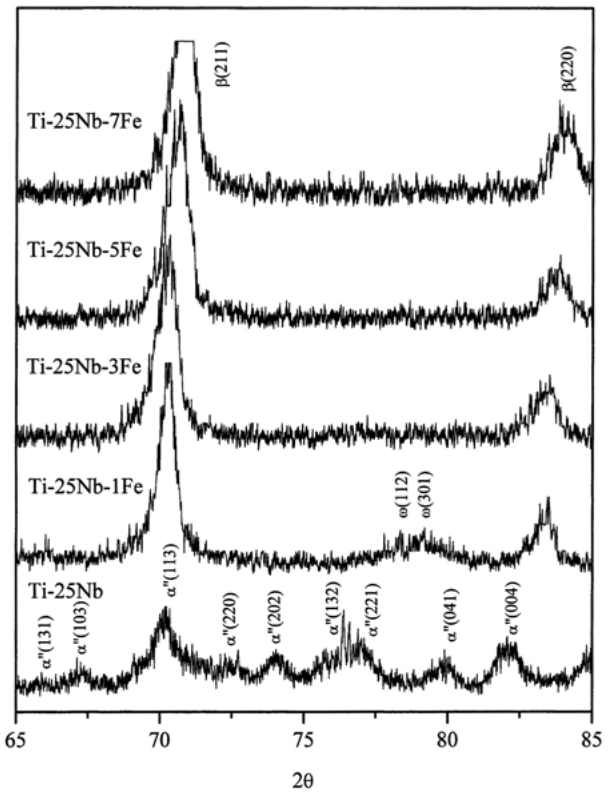

Figure 2 Low scanning speed XRD patterns of Ti–25Nb and Ti–25Nb–*x*Fe alloys.

The presence of ω phase could be more easily detected in lower scanning speed ($0.5^\circ\,min^{-1}$) XRD patterns. As shown in Fig. 2, when 1 wt % Fe was added, ω phase was present. For higher Fe contents, ω phase was no longer observed. The formation of ω phase in quenched Ti and Zr alloys has been reported in the early work of Bargariatskii *et al*. [26], Williams [27] and Balcerzak *et al*. [28]. As will be shown later, the presence of ω phase had a marked effect on mechanical properties of the present alloys.

Optical micrographs of cast c.p. Ti and the series of Ti–25Nb–*x*Fe alloys are shown in Fig. 3. The cast c.p. Ti exhibited a typical rapidly-cooled platelet-like morphology (Fig. 3(a)), while the binary Ti–25Nb alloy showed a needle-like α″ martensitic structure (Fig. 3(b)), similar to that observed in other Ti alloys [24, 29]. All iron-added alloys were comprised entirely of equi-axed, retained β phase grains (Figs. 3(c)–(f)). Apparently, when iron was added, the Ms temperature became lower than room temperature and the martensitic transformation was suppressed. The more profound dendritic structure observed in higher iron alloys is believed due to a solute-enhanced constitutional supercooling effect.

Microhardness and bending property data of the present Ti–25Nb and the series of Ti–25Nb–*x*Fe alloys are compiled in Table III. Properties of a c.p. Ti and Ti–6Al–4V are also listed for comparison. As shown in Fig. 4, the microhardness values of all present Ti–25Nb and Ti–25Nb–*x*Fe alloys (323.3–366.59 HV) were much higher than that of c.p. Ti (191.6 HV). The microhardness of α″ phase-dominated binary Ti–25Nb alloys was 323.3 HV. When 1 wt % iron was added, the microhardness increased to 341.6 HV. When 3 or 5 wt % iron was added, the microhardness decreased to a level similar to that of the binary Ti–25Nb alloy. The local maximum at 1 wt % Fe is believed to be a direct result of the presence of ω phase at this particular composition, as shown earlier in Fig. 2. When 7 wt % Fe was added, the microhardness increased again probably due to a solution hardening effect. The local maximum in microhardness at 1 wt % Fe was also occurred in the measurement of bending strength (Fig. 5). Again, this is believed to be a result of the strengthening/hardening effect of ω phase. According to an early study of Silcock [30], the slip in β titanium occurs predominantly in [1 1 1] direction on a number of slip planes. For slip in a given $[1\,1\,1]_\beta$ direction, only one of the four ω orientations has the close packed (0 0 0 1) direction favorably orientated, while the other three ω orientations have irrational directions parallel to $[1\,1\,1]_\beta$ and hence act as barriers to slip. The athermal ω-related increases in hardness in a number of Ti alloys were also observed by Bargariastkii *et al*. [26].

The iron effect on bending modulus was rather unexpected. As shown in Fig. 6, the binary Ti–25Nb alloy had a bending modulus (77 GPa) much lower than that of c.p. Ti (97.5 GPa) or Ti–6A1–4V (107 GPa). When 1, 5 or 7 wt % Fe was added, the bending modulus increased to 82–84 GPa. However, when 3 wt % Fe was added, the bending modulus of the alloy largely decreased to 70 GPa. Although this is not fully understood it seems that several different mechanisms, such as phase effect and solute effect, are competing to determine modulus of the alloy. It is generally accepted that the presence of ω phase increases hardness, strength and modulus of titanium alloy. While it is also generally accepted that the presence of β or α″ phase can effectively decrease modulus, the comparison in effectiveness between these two phases is rather inconclusive. In their recent study of binary Ti–Mo alloys Ho *et al*. [29] found that the alloy dominated by α″ phase had a lower modulus than that dominated by β phase. The present results, however, indicate that in the present Ti–25Nb–*x*Fe system the β phase alloy with low iron content and without ω phase (Ti–25Nb–3Fe) had the lowest modulus. As indicated in Table III, this particular composition results in a bending strength/modulus ratio as large as 24.6, that is higher than that of Ti–25Nb alloy (21.4) by 15%, than Ti–6Al–4V (17.4) by 41.4% and than c.p. Ti (9.3) by 165%. The high strength/modulus ratio of Ti–25Nb–3Fe alloy demonstrates its advantage for use as an implant material.

OCP and critical anodic current density values (determined from potentiodynamic polarization profiles) of Ti–25Nb and the series of Ti–25Nb–*x*Fe alloys are given in Table IV. All rest potentials became stable within 15 000 s. The potentiodynamic polarization tests showed that all present Ti–25Nb and Ti–25Nb–*x*Fe alloys had an excellent resistance to corrosion in Hank's physiological solution at 37 °C. Breakdown was never observed to occur to any alloy even at potentials as high as 3000 mV (SCE). Since this potential is much higher than the highest possible corrosion potential in the oral environment (-550 to $+400$ mV vs. Ag/AgCl or approximately -500 to $+450$ mV vs. SCE) [31], breakdown of these alloys in oral or body environment seems very unlikely to occur. In addition, it was reported

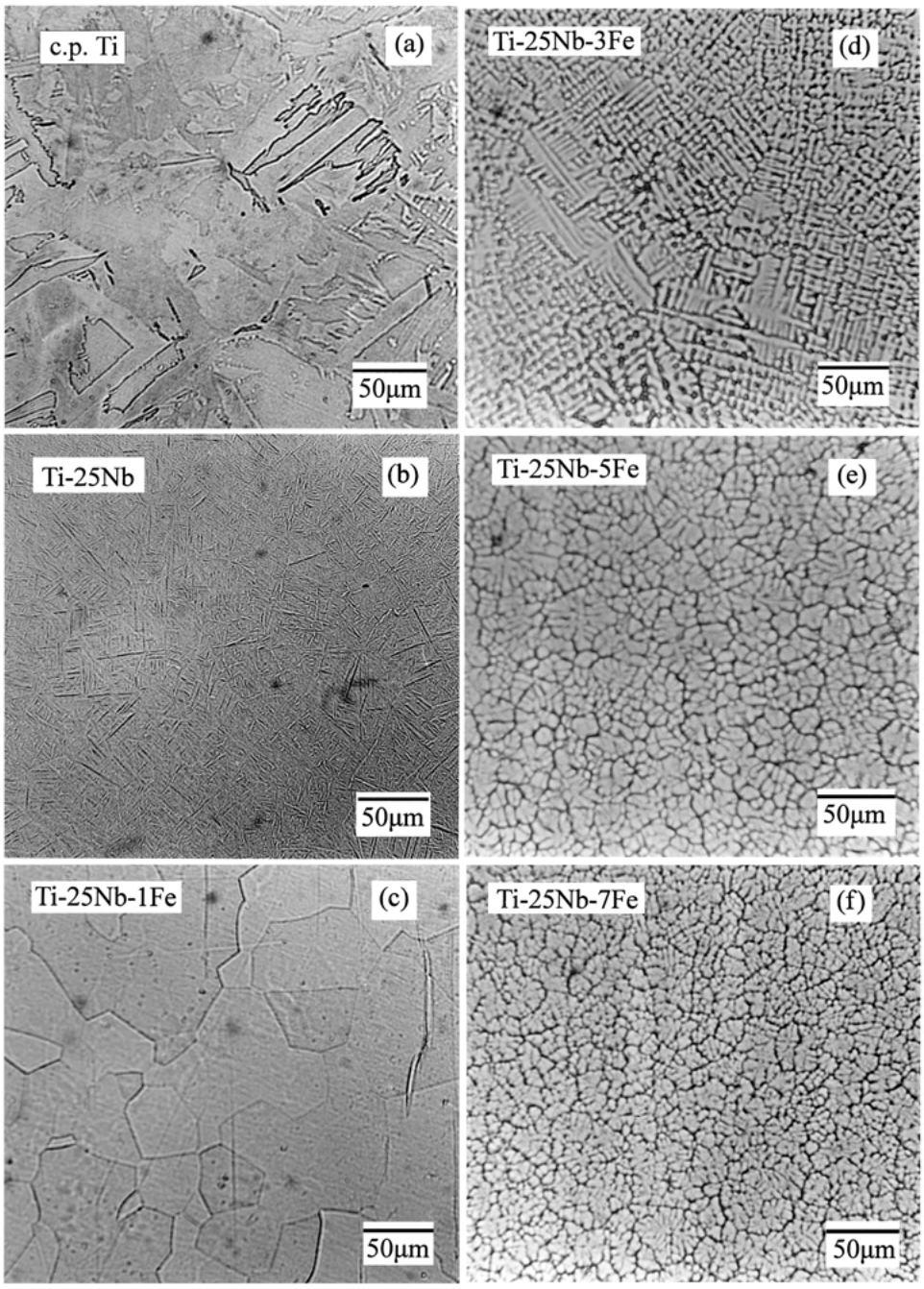

Figure 3 Optical micrographs of Ti–25Nb and Ti–25Nb–*x*Fe alloys.

that when an active–passive metal was exposed to an aerated corrosive medium and the critical anodic current density of the metal was lower than approximately 100 μA/cm^2 the metal would spontaneously passivate [32]. The low critical anodic current densities of the present alloys (almost an order of magnitude lower than 100 μA/cm^2) suggest that these alloys should easily be passivated in human body environment.

TABLE III Microhardness and bending properties

Alloy code	Microhardness (HA)	Bending strength (MPa)	Bending modulus (GPa)	Strength/ modulus ratio
c.p. Ti	323.3	910	97.5	9.3
Ti–6Al–4V	341.6	1863	107	17.4
Ti–25Nb	323.9	1650	77	21.4
Ti–25Nb–1Fe	329.7	1776	82	21.7
Ti–25Nb–3Fe	366.6	1699	70	24.6
Ti–25Nb–5Fe	188.3	1770	82	21.6
Ti–25Nb–7Fe	350.7	1804	84	21.5

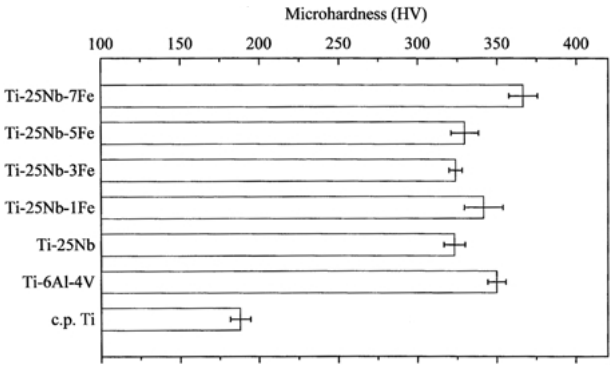

Figure 4 Microhardness of c.p. Ti, Ti–6Al–4V and various Ti–Nb–Fe alloys.

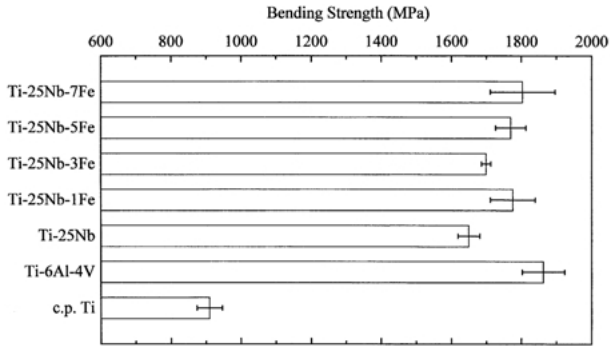

Figure 5 Bending strength of c.p. Ti, Ti–6Al–4V and various Ti–Nb–Fe alloys.

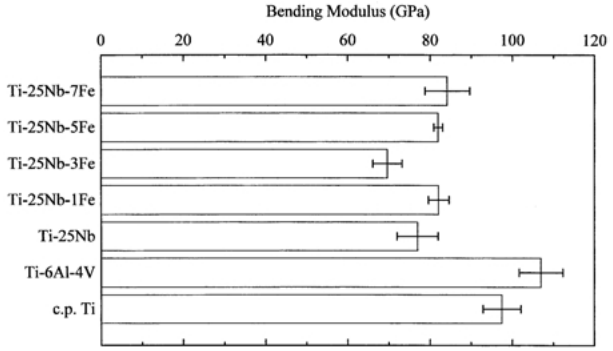

Figure 6 Bending modulus of c.p. Ti, Ti–6Al–4V and various Ti–Nb–Fe alloys.

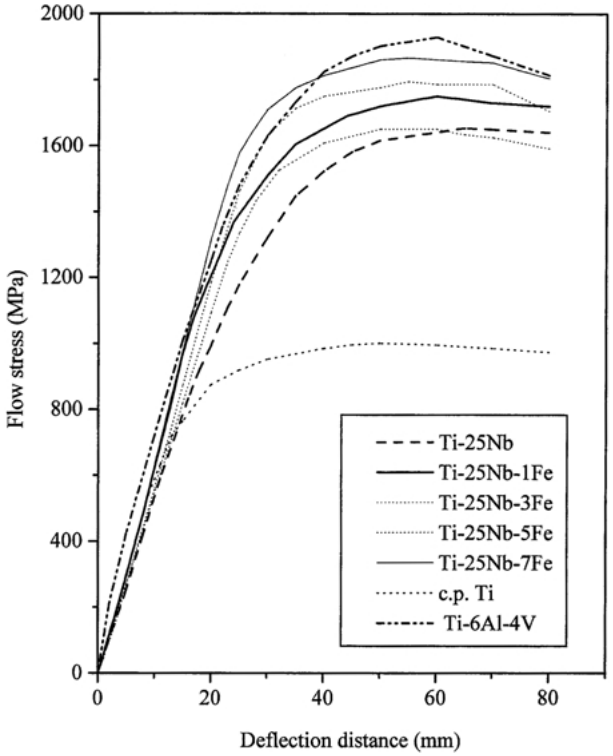

Figure 7 Typical bending stress-deflection profiles of Ti–25Nb and Ti–25Nb–*x*Fe alloys.

TABLE IV OCP and corrosion currents of Ti–25N and Ti–25Nb–*x*Fe alloys

Alloy code	I ($\mu A/cm^2$)	OCP (mV)
Ti–25Nb	2.1	− 50.3
Ti–25Nb–1Fe	1.9	− 4.6
Ti–25Nb–3Fe	6.6	− 8.1
Ti–25Nb–5Fe	1.4	− 47.2
Ti–25Nb–7Fe	0.35	− 93.8

4. Conclusions

1. Binary Ti–25Nb alloy showed a typical orthorhombic, α'' crystal structure. When 1 wt % or more iron was added, the formation of α'' phase was suppressed and β phase was retained. Only in Ti–25Nb–1Fe alloy was observed ω phase.

2. Binary Ti–25Nb alloy had a needle-like α'' martensitic structure. All iron-added alloys were comprised entirely of equi-axed, retained β phase grains.

3. When 1 wt % Fe was added to the alloy, both microhardness and bending strength values reached their local maxima. When 1, 5 or 7 wt % Fe was added, the bending modulus increased. Only when 3 wt % Fe was added, the bending modulus largely decreased. Ti–25Nb–3Fe alloy exhibits a bending strength/modulus ratio higher than that of Ti–25Nb alloy by 15%, than Ti–6A1–4V by 41.4% and than c.p. Ti by 165%.

4. All present Ti–25Nb and Ti–25Nb–*x*Fe alloys had an excellent resistance to corrosion in Hank's physiological solution at 37 °C. Breakdown never occurred to any alloy even at potentials as high as 3000 mV (SCE).

References

1. R. T. BOTHE, K. E. BEATON and H. A. DAVENPORT, *Surg. Gynecol. Obstet.* **71** (1940) 598.
2. P. I. BRANEMARK, R. ADELL and T. ALBREKTSSON, *Adv. Biomater.* **4** (1982) 133.
3. S. RAO, T. USHIDA, T. TATEISHI, Y. OKAZAKI and S. ASAO, *Bio-Med. Mater. Engng.* **6** (1996) 79.
4. P. R. WALKER, J. LEBLANC and M. SIKORSKA, *Biochemistry* **28** (1990) 3911.
5. D. R. C. MCLACHLAN, B. FARNELL and H. GALIN, in ''Biological Aspects of Metals and Metal-Related Disease'' (Ravon Press, New York, 1983) p. 209.
6. S. YUMOTO, H. OHASHI, H. NAGAI, S. KAKIMI, Y. OGAWA, Y. IWATA and K. ISHII. *Int. J. PIXE.* **2** (1992) 493.
7. Y. OKAZAKI, Y. ITO, A. ITO and T. TATEISHI, in ''Medical Applications of Titanium and Its Alloys: The Material and Biological Issues'' (Proceedings of a symposium held in 1994 in Phoenix, Arizona) edited by S. A. Brown and J. E. Lemons (ASTM, West Conshohocken, 1996) p. 45.
8. A. K. MISHRA, J. A. DAVIDSON, R. A. POGGIE, P. KOVACS and T. J. FITZGERALD, in ''Medical Applications of Titanium and Its Alloys: The Material and Biological Issues'' (Proceedings of a symposium held in 1994 in Phoenix, Arizona) edited by S. A. Brown and J. E. Lemons (ASTM, West Conshohocken, 1996) p. 96.
9. K. K. WANG, L. J. GUSTAVSON and J. H. DUMBLETON, in ''Medical Applications of Titanium and Its Alloys: The Material and Biological Issues'' (Proceedings of a symposium held in 1994 in Phoenix, Arizona) edited by S. A. Brown and J. E. Lemons (ASTM, West Conshohocken, 1996) p. 76.
10. L. D. ZARDIACKAS, D. W. MITCHELL and J. A. DISEG, in ''Medical Applications of Titanium and Its Alloys: The Material

and Biological Issues'' (Proceedings of a symposium held in 1994 in Phoenix, Arizona) edited by S. A. Brown and J. E. Lemons (ASTM, West Conshohocken, 1996) p. 60.
11. J. A. DAVIDSON, U.S. Patent No. 5954724, 1999.
12. MARC LONG, H. J. RACK, *Biomaterials* **19** (1998) 1621.
13. D. KURODA, M. NIINOMI, M. MORINAGA, Y. KATO and T. YASHIRO, *Mater. Sci. Engng.* **A243** (1998) 244.
14. A. R. DUJOVNE, J. D. BOBYN, J. J. KRYGIER, J. E. MILLER and C. E. BROOKS, *J. Arthroplasty.* **8** (1993) 7.
15. C. A. ENGH and J. D. BOBYN, *Orthop. Relat. Res.* **231** (1988) 7.
16. D. R. SUMNER and J. O. GALANTE, *Clin. Orthop. Relat. Res.* **274** (1992) 202.
17. K. IDA, *Quintessence* **2** (1983) 114.
18. A. SARMIENTO, G. A. ZYCH, L. L. LATTA and R. R. TARR, *Clin. Orthop.* **144** (1979) 166.
19. M. F. SEMLITSCH, H. WEBER, R. M. STREICHER and R. SCHON, *Biomaterials* **13** (1992) 781.
20. E. CHEAL, M. SPECTOR and W. HAYES, *J. Orthop. Res.* **12** (1990) 379.
21. P. PRENDERGAST and D. J. TAYLOR, *Biomed. Engng.* **12** (1990) 379.
22. J. D. BOBYN, A. H. GLASSMAN, H. GOTO, J. KRYGIER, J. J. MILLER and C. E. BROOKS, *Clin. Orthop. Relat. Res.* **261** (1990) 196.
23. J. D. BOBYN, E. S. MORTIMER, A. H. GLASSMAN, C. A. ENGH, J. J. MILLER and C. E. BROOKS, *ibid.* **274** (1992) 79.
24. C. M. LEE, J. H. CHERN LIN and C. P. JU, *J. Oral Reh.* (accepted).
25. A. GUHA, in ''Metals Handbook'' (American Society for Metals, Metals Park, Ohio, 1985) p. 133.
26. I. A. BAGARIATSKII, G. I. NOSOVA and T. V. TAGUNOVA, *Sov. Phys.: Doklady Engl. Transl.* **3** (1959) 1014.
27. J. C. WILLIAMS, in ''Titanium Science and Technology; Proceeding. Metallurgical Society of AIME'' (Plenum Press, New York, 1973) p. 1433.
28. A. T. BALCERZAK and S. L. SASS, *Metall. Trans.* **3** (1972) 1601.
29. W. F. HO, C. P. JU and J. H. CHERN LIN, *Biomaterials* **20** (1999) 2115.
30. J. M. SILCOCK, *Acta Metallurgica* **6** (1958) 481.
31. M. BERGMAN, O. GINSTRUP and B. NILLSON, *Scandinavian J. Dent. Res.* **90** (1982) 331.
32. M. G. FONTANA, in ''Corrosion Engineering'' (McGraw-Hill, New York, 1986) p. 493.

Received 23 May
and accepted 23 October 2001